VascularBiology

Vascular Biology (2025) **7** e230013
https://doi.org/10.1530/VB-23-0013

Received 19 June 2023
Accepted 14 January 2025
Available online 15 January 2025
Version of Record published 29 January 2025

RESEARCH

Lack of intracranial atherosclerosis in various atherosclerotic mouse models

Diewertje I Bink[1], Katja Ritz[1], Claire Mackaaij[1], Olga Stam[1], Sanny Scheffer[1], Mark R Mizee[2], Hanneke J Ploegmakers[1], Bert J van het Hof[2], Onno J de Boer[1], Judith C Sluimer[3], Guido R Y De Meyer[4], Louise van der Weerd[5,6], Helga E de Vries[2] and Mat J A P Daemen[1]

[1]Department of Pathology, Amsterdam UMC, Academic Medical Center Amsterdam, The Netherlands
[2]Department of Molecular Cell Biology and Immunology, Amsterdam Neuroscience, Amsterdam UMC, Amsterdam, The Netherlands
[3]Department of Pathology, CARIM, Maastricht University Medical Center, Maastricht, The Netherlands
[4]Laboratory of Physiopharmacology, University of Antwerp, Antwerp, Belgium
[5]Department of Radiology, Leiden University Medical Center, Leiden, The Netherlands
[6]Department of Human Genetics, Leiden University Medical Center, Leiden, The Netherlands

Correspondence should be addressed to D I Bink: d.bink1@amsterdamumc.nl

Abstract

Although mice are used extensively to study atherosclerosis of different vascular beds, limited data are published on the occurrence of intracranial atherosclerosis. Since intracranial atherosclerosis is a common cause of stroke and is associated with dementia, a relevant animal model is needed to study these diseases. We examined the presence of intracranial atherosclerosis in different atherogenic mouse strains and studied differences in vessel wall characteristics in mouse and human tissue in search of possible explanations for the differing atherosclerotic susceptibility between extracranial and intracranial vessels. The presence of atherosclerotic plaques was systematically examined from the distal common carotids to the circle of Willis in three atherogenic mouse models. Extra- and intracranial vessel characteristics were studied by immunohistochemistry. All three strains developed atherosclerotic lesions in the common carotids, while no lesions were found intracranially. This coincided with altered vessel morphology. Compared to extracranial sections, intracranially the number of elastic layers decreased, tight junction markers increased, and antioxidant enzyme heme oxygenase (HO)-1 increased. Higher HO-1 expression was also shown in human intracranial arteries. Human brain endothelial cell stimulation with oxidized LDL induced endogenous protective antioxidant HO-1 levels through NRF2 translocation. Intracranial atherosclerosis was absent in three atherogenic mouse models. Intracranial vessel segments showed an increased presence of junction markers in mice and increased HO-1 in both mice and human tissue. We suggest that differences in brain vessel structure and induced antioxidant levels in the brain endothelium found in mouse and human tissue may contribute to the decreased atherosclerosis susceptibility of intracranial arteries.

Keywords: atherosclerosis; mouse model; endothelial cells; circle of Willis; intracranial disease; anti-oxidant

Introduction

Intracranial atherosclerosis is the cause of at least 10% of ischemic strokes and is associated with dementia (1, 2, 3). The prevalence of intracranial atherosclerosis varies by ethnicity and increases from about 23% of the population at ages 50–59 to 80% at ages 80–89 (4). It becomes increasingly clear that distinct vessel and atherosclerotic plaque characteristics of intra- and extracranial arteries are observed in humans (5). Intracranial atherosclerosis develops approximately 20 years later compared to coronary or carotid

Published by Bioscientifica Ltd.
https://vb.bioscientifica.com

Vascular Biology (2025) **7** e230013
https://doi.org/10.1530/VB-23-0013

atherosclerosis and shows a more stable and less severe phenotype than extracranial atherosclerosis. The underlying mechanisms of these striking differences are largely unknown, but they may be related to a specific constitution of intracranial vessels as observed in different species (5). For example, intracranial vessels have fewer elastic fibers than extracranial vessels, a distinct vessel wall metabolism and glycocalyx composition, elevated endogenous antioxidant enzyme activity, a lower expression of inflammatory genes and more tight junctions between the endothelial cells lining the vessel wall (5, 6, 7, 8). In addition, a reduction in vessel wall permeability and lipoprotein deposition in the vessel wall of intracranial arteries compared to extracranial arteries has been observed in monkeys and rabbits (6, 7).

Only few studies have been published on the occurrence and frequency of atherosclerotic plaques within the skull or brain of experimental animals. Large animals such as dogs, monkeys and swine develop visible intracranial atherosclerotic lesions (9, 10, 11). However, small-sized animals, such as rats and rabbits, only develop lesions with intimal thickening and foam cell formation in the intracranial vessel wall (12, 13, 14, 15, 16). In mice, the presence of intracranial atherosclerosis in the circle of Willis (CoW) has been stated in the crossbreed of LDLr$^{-/-}$ with hApoB expression on a chow diet; however, no quantitative data on plaque size or phenotype were shown (17). The absence of intracranial atherosclerosis in the CoW was reported in 80-week-old ApoE$^{-/-}$LDLr$^{-/-}$ mice and 18-month-old ApoE$^{-/-}$ mice on western-type diet (WD) (18, 19). In addition, the absence of intracranial atherosclerosis has been reported in ApoE$^{-/-}$ mice in the middle cerebral artery (MCA) and basilar artery (BA) at the age of 29 weeks, in the cerebral arterioles at the age of 7–13 months on WD, and in cerebral microvessels at the age of 8–10 months on chow (20, 21, 22). In the latter, lipid-laden macrophages were observed in the perivascular region, indicating that hypercholesterolemia does affect the brain in these mice, but these changes do not progress in the vascular wall.

To determine the presence or absence of intracranial atherosclerosis in atherosclerotic mice, we collected the heads of three atherosclerotic mouse models (ApoE$^{-/-}$ mice, ApoE$^{-/-}$Fbn1$^{C1039G+/-}$ and ApoB100/LDLr$^{-/-}$ mice) that had already been used in other studies. Intracranial vessels were systematically analyzed for the presence of atherosclerosis. Moreover, the precise transition point from atherosclerotic to non-atherosclerotic vessel areas was also determined. To determine the plausible causes of the reduced susceptibility of intra- and extracranial arteries, we studied structural intra- and extracranial vessel wall characteristics in young ApoE$^{-/-}$ and C57Bl/6 mice, prior to the age when they developed atherosclerotic plaques. Because differences were found in the amount of antioxidant enzyme staining in both mouse strains, we also determined differences in antioxidant enzyme expression in human intracranial and extracranial arteries and studied changes in the antioxidant levels in cultured human brain endothelial cells upon oxidized LDL (oxLDL) stimulation, mimicking pro-atherosclerotic conditions.

Materials and methods

An expanded Materials and methods section is available in Supplementary material online (see section on Supplementary materials given at the end of the article).

Animals

Thirty-three mice from three genetically modified mouse models were obtained from different laboratories to study the presence of atherosclerosis. Four ApoE$^{-/-}$ on a chow diet at the age of 50–52 weeks (M and F), eight ApoE$^{-/-}$ on a WD at the age of 28–41 weeks (M and F), 12 ApoE$^{-/-}$Fbn1$^{C1039G+/-}$ on a WD at the age of 21–41 weeks (F) and eight ApoB100/LDLr$^{-/-}$ mice (M and F) ranging from 37–41 weeks of age (also shown in Table 1). ApoE$^{-/-}$ and ApoE$^{-/-}$Fbn1$^{C1039G+/-}$ were fed a WD from 6 weeks of age, hApoB100/LDLr$^{-/-}$ female mice from 12 weeks of age and ApoB100/LDLr$^{-/-}$ male mice from 32 weeks of age until sacrifice. For all ApoE$^{-/-}$ and ApoE$^{-/-}$Fbn1$^{C1039G+/-}$ mice, the complete head and neck, including the vascular tree, were retrospectively harvested from other experimental studies and complemented with ApoB100/LDLr$^{-/-}$ mice, leading to differences in age and diet between the experimental groups (23). Differences in ages also occurred due to premature death (Table 1). In addition, seven 10-week-old ApoE$^{-/-}$ and six 16-week-old C57Bl/6 chow-fed mice were used for immunohistochemical analyses.

All studies were approved by the local ethical committee of the University of Antwerp, the animal welfare committee of the LUMC and the regulatory authority of MUMC and were performed in accordance with national and European regulations.

MRI

A magnetic resonance angiogram of one mouse was made as an anatomical reference. The vasculature segmentation was done with AMIRA (version 9.0; https://www.thermofisher.com/nl/en/home/electron-microscopy/products/software-em-3d-vis/amira-software.html).

CT

A CT scan was performed for a three-dimensional overview of the vascular tree and its entry into the skull for one mouse. Vasculature and bone segmentation were done with AMIRA (version 9.0).

Vascular Biology (2025) **7** e230013
https://doi.org/10.1530/VB-23-0013

Table 1 Presence of atherosclerotic lesions in individual mice of the three investigated atherogenic mouse strains.

				Extracranial					Intracranial		
Mouse model	**Gender**	**Age**	**Diet**	**CCA**	**ECA**	**ICA**	**Ptgpal**	**VA**	**ICA**	**CoW**	**BA**
ApoE$^{-/-}$	M	50w	Chow	✓	✓	-	-	-	-	-	-
ApoE$^{-/-}$	F	52w	Chow	✓	✓	✓	✓	-	-	-	-
			Chow	✓	✓	✓	✓	-	-	-	-
			Chow	✓	✓	✓	✓	-	-	-	-
ApoE$^{-/-}$	M	28w	WD	✓	✓	✓	-	-	-	-	-
			WD	✓	✓	✓	✓	-	-	-	-
ApoE$^{-/-}$	F	41w	WD	✓	✓	✓	✓	-	-	-	-
			WD	✓	✓	✓	✓	-	-	-	-
			WD	✓	✓	✓	✓	-	-	-	-
			WD	✓	✓	✓	✓	-	-	-	-
			WD	✓	✓	✓	✓	✓	-	-	-
			WD	✓	✓	✓	✓	✓	-	-	-
ApoE$^{-/-}$Fbn1$^{C1039G\ \pm}$	F	21w	WD	✓	✓	✓	✓	-	-	-	-
		26w	WD	✓	✓	✓	✓	-	-	-	-
			WD	✓	✓	✓	✓	-	-	-	-
			WD	✓	✓	✓	✓	-	-	-	-
			WD	✓	✓	✓	✓	✓	-	-	-
			WD	✓	✓	✓	✓	-	-	-	-
		27w	WD	✓	✓	✓	✓	-	-	-	-
			WD	✓	✓	✓	✓	-	-	-	-
		29w	WD	✓	✓	✓	✓	✓	-	-	-
		31w	WD	✓	✓	✓	✓	-	-	-	-
		41w	WD	✓	✓	✓	✓	-	-	-	-
			WD	✓	✓	✓	✓	✓	-	-	-
ApoB100/LDLr$^{-/-}$	F	37w	WD	✓	✓	✓	✓	-	-	-	-
			WD	✓	✓	✓	✓	-	-	-	-
			WD	✓	✓	✓	✓	-	-	-	-
			WD	✓	✓	✓	✓	-	-	-	-
	M	41w	WD	✓	✓	✓	✓	✓	-	-	-
			WD	✓	✓	✓	✓	-	-	-	-
			WD	✓	✓	✓	✓	-	-	-	-
			WD	✓	✓	✓	✓	-	-	-	-

ApoB: apolipoprotein B; ApoE, apolipoprotein E; BA, basilar artery; CCA, common carotid artery; CoW, circle of Willis; ECA, external carotid artery; F, female; Fbn1, Fibrillin-1; ICA, internal carotid artery; LDLr, low-density lipoprotein receptor; M, male; Ptgpal, pterygopalatine artery; VA, vertebral artery; WD, western-type diet.

Histology and immunohistochemistry

Mice were sacrificed by transcardial perfusion. Sections of atherogenic mice were cut at 10 μm thickness, and every fifth section was stained with hematoxylin and eosin (HE) to assess the distribution of atherosclerotic lesions, ranging from foam cell detection in the vessel wall to advanced atherosclerotic plaques, as defined by the AHA classification (24, 25). Lesions at the common carotid artery (CCA) bifurcation were classified according to the AHA classification.

The skulls of seven non-perfused, 10-week-old ApoE$^{-/-}$ mice and six 16-week-old C57Bl/6 mice were decalcified and cut transversely at 5 μm thickness for immunofluorescence (IF) (ApoE$^{-/-}$) or immunohistochemical (C57Bl/6) analysis of vessel characteristics and morphology. HE stainings were used to determine seven areas of interest (see Fig. 1B): just below the CCA bifurcation (no. 1), the internal carotid artery (ICA) before the bifurcation with the pterygopalatine artery (Ptgpal) (no. 2), the ICA after the bifurcation with the Ptgpal (no. 3), the ICA just below the skull base (no. 4), the ICA within the skull base (no. 5), the ICA just above the skull base (no. 6) and the ICA at the start of circle of Willis (CoW) before the bifurcations to the posterior cerebral artery and MCA (no. 7). Adjacent sections were used for Elastica van Gieson (EvG) staining and IF or immunohistochemistry, using antibodies listed in Supplemental Tables 1 and 2.

Human paraffin-embedded samples of the CCAs and BA, obtained from 16 autopsy patients, were used to perform IF and confocal microscopy.

Double stains were performed by combining CD31, an endothelial cell marker, with one of the following oxidative stress markers HO (heme oxygenase)-1, eNOS and NRF2. The dilutions used are shown in Supplemental Table 4.

Vascular Biology (2025) **7** e230013
https://doi.org/10.1530/VB-23-0013

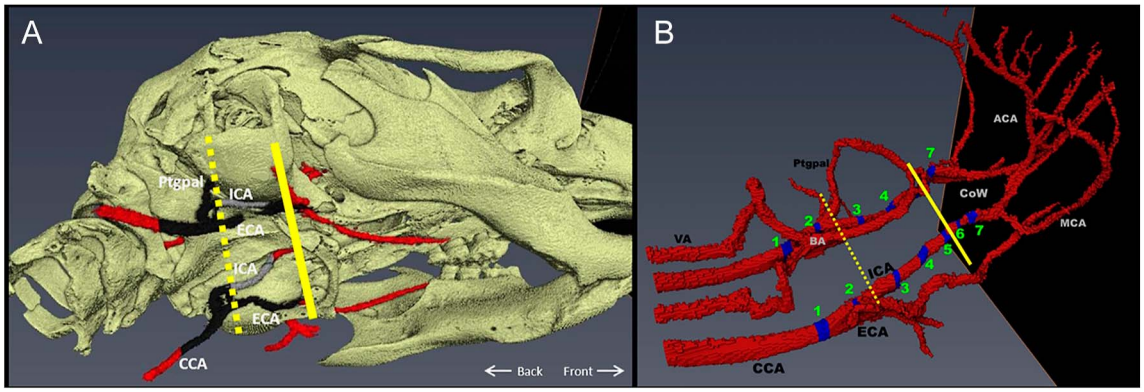

Figure 1

Three-dimensional reconstruction of the peripheral and cerebral arterial tree. (A) CT scan showing a slightly ventrolateral view of the skull and vessels. The dashed line indicates where the atherosclerotic plaques stop in most mice. The continuous line indicates the place where the internal carotid artery (ICA) enters the skull. Red indicates parts of the vessels without atherosclerosis. Black indicates the parts of the vessels with extensive atherosclerosis (based on 32 mice). Gray indicates atherosclerosis as observed in only one mouse. (B) Magnetic resonance angiogram showing the sagittal view of the mouse arterial tree from common carotid artery (CCA) to the circle of Willis (CoW) and its main branches. The numbered blue areas indicate the areas in which immunohistochemistry sections were taken.

Image analysis

Image acquisition of the IF-stained ApoE$^{-/-}$ mouse skulls and human FFPE samples was performed on a Leica TCS SP8 X confocal microscope (Leica Microsystems, Germany). The outline of the positive area in the CD31-stained pictures was used to determine the region of interest. Within this region, the fluorescence intensity for the oxidative stress markers was assessed.

Bright-field image acquisition of the HE, EvG and immunohistochemistry stainings was taken using a Leica DM5000B microscope (Leica, Germany). Image analysis was performed to determine the optical density (OD) for PermaBlue-stained IHC and the percent positive area. The vessel wall intima and media were selected as regions of interest (right and left arteries averaged). Vessel wall thickness was measured on the HE-stained sections.

Cell culture and treatments

The immortalized human brain endothelial cell line hCMEC/D3 was cultured as described previously (26, 27). Cells were treated with human oxLDL (BT-910, Biomedical Technologies Inc., USA). Uptake of oxLDL was confirmed with Dil-oxLDL (BT-920, Alfa Aesar, USA) and FACS analysis, and quenching for surface fluorescence was confirmed with Trypan blue.

RNA isolation and real-time quantitative PCR

hCMEC/D3 cells were stimulated for 6 and 24 h with 50 and 100 μg/mL oxLDL (n = 4), harvested using TRIzol reagent (Invitrogen, USA) followed by the RNA isolation. cDNA synthesis was performed with 1 μg RNA. cDNA was amplified using SYBR Green with primers against HO-1 primers and beta-2-microglobulin and the $2-\Delta\Delta CT$ method was used for data analysis (28).

Western blotting and nuclear fractioning

To determine HO-1 protein levels using western blotting, hCMEC/D3 cells were stimulated for 24 h with oxLDL (n = 3). Cells were lysed in cell lysis buffer (Cell Signaling Technology Inc, USA), taken up in SDS sample buffer and heated to 95 °C for 5 min. Lysates were resolved on a 10% SDS–polyacrylamide gel electrophoresis, blotted to PVDF membranes (Bio-Rad Laboratories, USA) and incubated O/N at 4 °C with primary antibodies against HO-1 and actin for 1 h at RT. Respective IRDye infrared fluorescent dyes secondary antibodies and the Odyssey infrared imaging system (Li-COR) were used for visualization and quantification of protein levels.

To determine NRF2 nuclear protein levels, hCMEC/D3 cells were stimulated for 4 h with oxLDL (n = 3). Cells were lysed and fractioned using the NE-PER nuclear and cytoplasmic extraction kit following the manufacturer's instructions (Thermo Scientific, USA). Western blotting was performed using primary antibodies against NRF2, lamin B and α-actin. Fluorescence intensity was measured in the area surrounding the protein bands and subtracted by the same area without bands for lane background correction. Relative NRF2 protein levels were obtained by correcting for loading control (actin or lamin B) levels in each sample.

Statistical analysis

Data were analyzed using Graphpad Prism software (v5.01, USA; https://www.graphpad.com).

Vascular Biology (2025) **7** e230013
https://doi.org/10.1530/VB-23-0013

Mouse immunohistochemical measures were considered statistically significant if $P < 0.05$ by Friedman test. Post hoc tests were done with Dunn's test to compare all pairs of columns. Human immunohistochemical measures were considered statistically significant if $P < 0.05$ determined by a Wilcoxon signed-rank test. *In vitro* results are shown as median ± standard deviation for FACS results and as means ± standard error of the mean for others. Statistical significance was considered if $P < 0.05$ by two-tailed Student's *t*-test.

Results

Mapping of the mouse arterial organization

Histological and immunohistochemical stainings of transversal mouse head sections were analyzed to detect the distribution of atherosclerotic plaques and the vessel wall characteristics. For the nomenclature of vessels, the rat anatomy atlas from Greene and the MRI results from Kara and coworkers were used (29, 30). For the assessment of atherosclerotic lesions, we focused on the CCA, proximal parts of the external carotid artery (ECA), ICA, pterygopalatine artery (Ptgpal), circle of Willis (CoW), vertebral artery (VA) and the BA (Fig. 1).

Atherosclerotic lesions are absent in the mouse cranium

The severity of the extracranial atherosclerotic lesions in ApoE$^{-/-}$, ApoE$^{-/-}$Fbn1$^{C1039G+/-}$ and ApoB100/LDLr$^{-/-}$ mice was classified at the CCA bifurcation (24, 25). Almost all mice showed predominantly advanced lesions, type V, according to the AHA classification: the lesions contained large necrotic cores, cholesterol crystals, layers of fibrous connective tissue and macrophage foam cells. Only one male ApoB100/LDLr$^{-/-}$ mouse showed less advanced lesions (type III).

While all 32 animals developed atherosclerotic lesions in at least one of the CCAs (Table 1), intracranial atherosclerotic lesions were completely absent. Atherosclerotic lesions were frequently present in the ICA cranial from the bifurcation with the CCA but typically stopped at the bifurcation with the Ptgpal, indicating a first transition point in atherosclerotic susceptibility (Figs 1A and 2). Only three ApoE$^{-/-}$Fbn1$^{C1039G+/-}$ mice out of all 32 mice showed early or advanced atherosclerotic lesions in the ICA after the ICA bifurcation with the Ptgpal; one of these showed lesions within the carotid foramen. However, there were no lesions in the ICA once it entered the cranial cavity, indicating a second transition point in atherosclerotic susceptibility between the extracranial and intracranial parts of the ICA. In six mice, lesions were observed in the extracranial portion of the VA but not in the intracranial part or in the BA (Table 1).

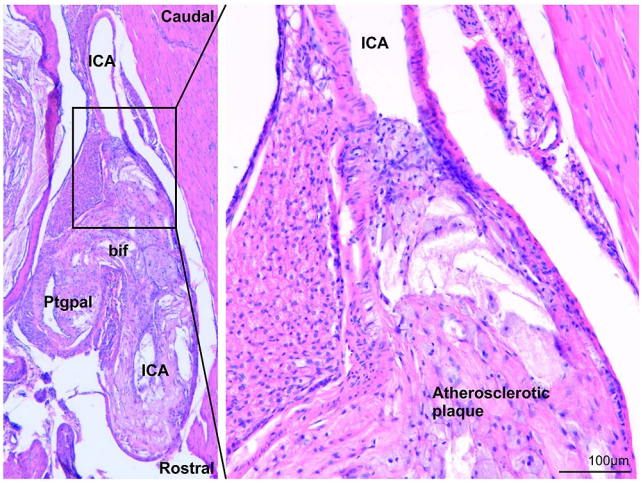

Figure 2

Representative picture of the first transition point of the internal carotid artery (ICA) at the bifurcation (bif) with the pterygopalatine artery (Ptgpal) where the atherosclerotic lesion usually stopped in a 26-week-old ApoE$^{-/-}$Fbn1$^{C1039G+/-}$ mouse on a WD. An atherosclerotic plaque containing a necrotic core with foamy macrophages is shown in the ICA on the rostral site of the bifurcation. There was no plaque at the cranial site of the bifurcation, the site of the vessel that is heading toward the brain. In the left panel (2.5×), an overview of the bifurcation of the ICA and Ptgpal is shown, while the right panel (10×) shows the first transition point in more detail.

Thus, none of the 32 mice showed intracranial atherosclerotic lesions, despite the advanced age of the mice and advanced atherosclerosis in extracranial arteries.

Although an older age may have increased the atherosclerotic burden, later time points were not achievable in the ApoB100/LDLr$^{-/-}$ mice on long-term WD, as they needed to be euthanized at 8.5 months of age because of large subcutaneous fat depositions in the paws and consequential muscle compression. Most ApoB100/LDLr$^{-/-}$ (n = 7/8), ApoE$^{-/-}$Fbn1$^{C1039G+/-}$ (n = 11/12) and ApoE$^{-/-}$ (n = 3/6) mice on WD had small to large xanthomas in their brains, mainly in and around the choroid plexus and neocortex, as shown by Van der Donckt and coworkers (23). Furthermore, ApoB100/LDLr$^{-/-}$ (n = 7/8), ApoE$^{-/-}$Fbn1$^{C1039G+/-}$ (n = 10/12) and ApoE$^{-/-}$ (n = 4/6) mice on WD and ApoE$^{-/-}$ (n = 2/4) mice on chow had cholesterol granulomas in their middle and inner ears, affecting surrounding tissue and blocking the perception of auditory signals.

Intra- and extra-cranial vessel wall characteristics differ

Next, we studied vessel wall characteristics in the intima and media that may be linked to the profound difference in the susceptibility of atherosclerosis development between extracranial and intracranial arteries in 10-week-old ApoE$^{-/-}$ mice before extracranial plaque

Vascular Biology (2025) **7** e230013
https://doi.org/10.1530/VB-23-0013

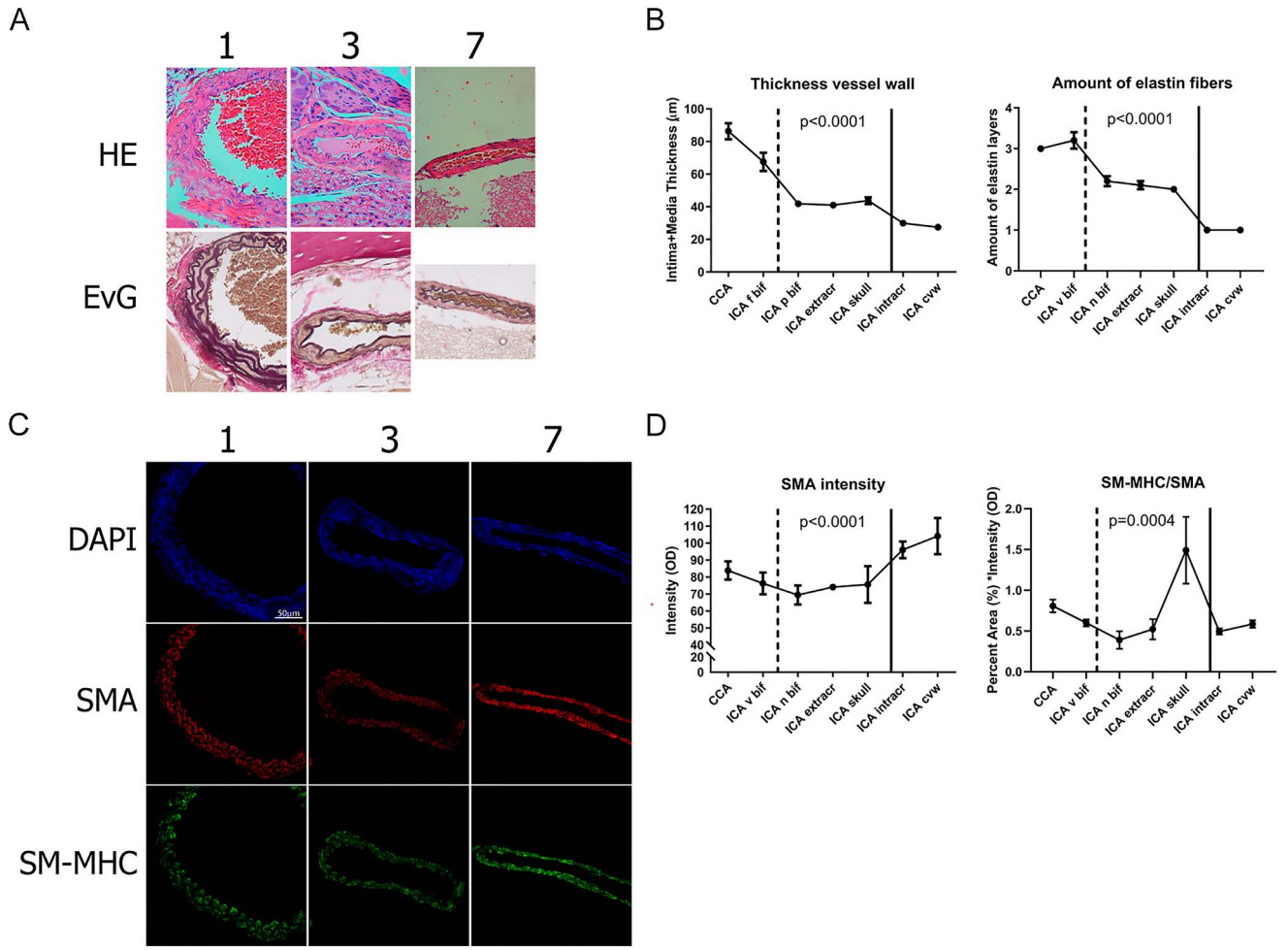

Figure 3

Changes in vessel wall characteristics in 10-week-old ApoE$^{-/-}$ mice on normal chow measured in seven artery segments from the common carotid artery (CCA, 1) to the extracranial part of the internal carotid artery (ICA, 3) and the intracranial part of the ICA (7). (A) Hematoxylin and eosin and EvG staining and (B) the quantification of the vessel wall thickness and amount of elastin layers (n = 5–7). (C) Example pictures of changes in SMA and SM-MHC staining. (D) Quantification of the amount of positive SMA and SM-MHC/SMA staining (n = 6–7). Statistical significance was determined by the Friedman test and considered statistically significant if $P < 0.05$.

development. Examples of the CCA, the extracranial ICA and the intracranial ICA are shown in Figs 3, 4, 5. The numbers in the figure and text indicate the locations where the sections for immunohistochemistry and IF were taken and are shown in Fig. 1B. Several differences in vessel wall characteristics were observed.

Intima-media thickness was determined in the HE stainings and was shown to decrease going from the extracranial CCA to the intracranial ICA ($P < 0.0001$) (Fig. 3A and B). With an EvG staining, the number of elastic lamina layers was assessed. The CCA (no. 1 in Fig. 1B) and ICA before the bifurcation with the Ptgpal (no. 2) showed 3–4 elastic lamina layers. Beyond the Ptgpal bifurcation (no. 3), the ICA contained only two elastica lamina layers. The intracranial part of the ICA showed a thick IEL and a discontinuous elastic layer in the media (nos 6 and 7) (Fig. 3A and B).

The relative amount of smooth muscle cells (SMCs) in the vessel wall and the differentiation level of the SMC's were measured with smooth muscle actin (SMA) and smooth muscle myosin heavy chain (SM-MHC), respectively. SM-MHC is a marker of mature contractile SMCs, its expression increases with the maturation of SMCs, and a lower amount is observed in atherosclerotic lesions (31). The percent-positive area and intensity of SMA increased intracranially, indicating a relative increase of SMCs in the vessel wall (area fraction $P = 0.0003$ and intensity $P < 0.0001$). SMC differentiation increased in the extra- and intracranial parts of the ICA when presented as percent area, but decreased when presented as intensity

Vascular Biology (2025) **7** e230013
https://doi.org/10.1530/VB-23-0013

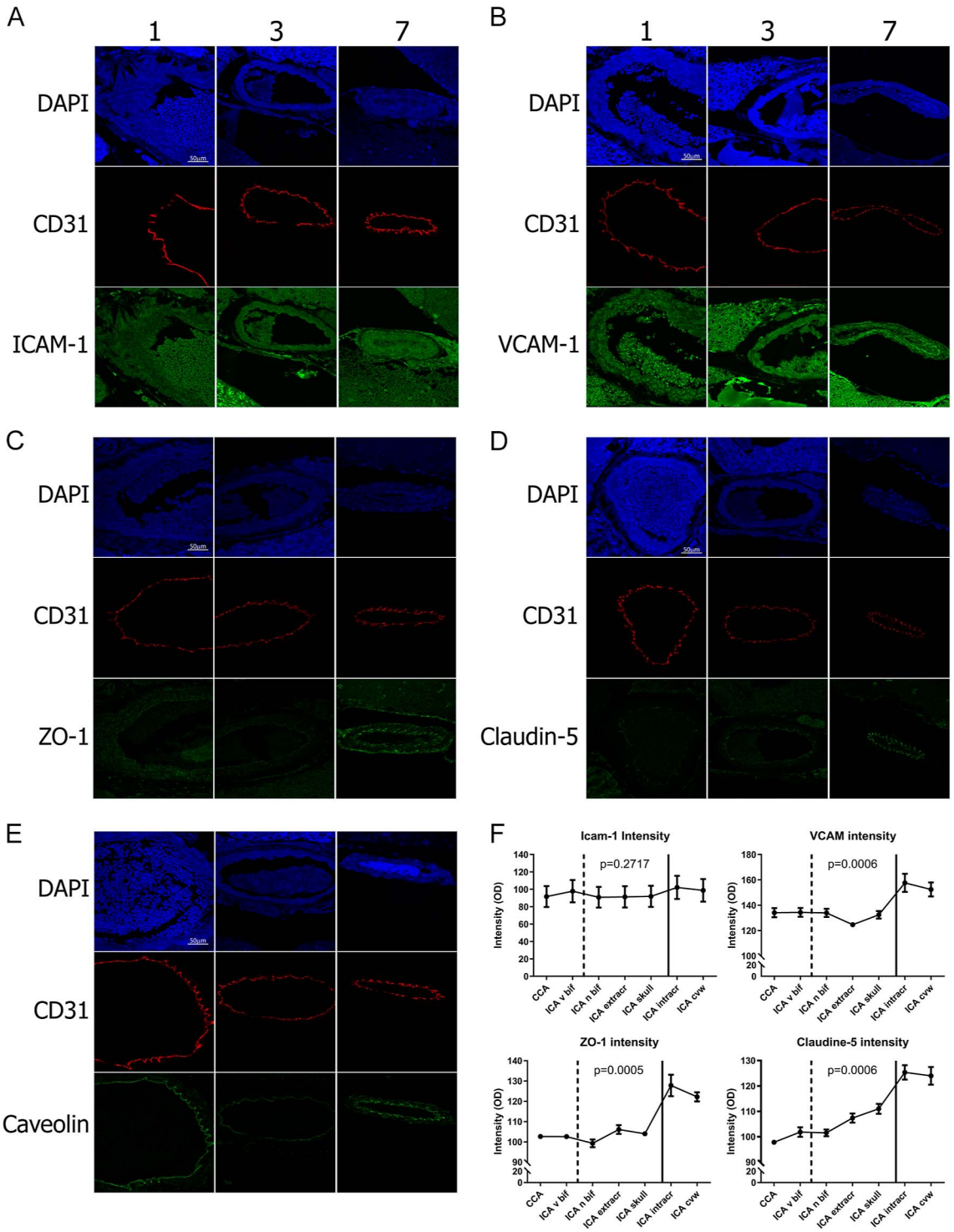

Figure 4

(A–E) Example pictures of changes in (A) ICAM-1, (B) VCAM-1, (C) ZO-1, (D) Claudin-5 and (E) Caveolin in 10-week-old ApoE$^{-/-}$ mice on normal chow stained in the common carotid artery (CCA, 1), the extracranial part of the internal carotid artery (ICA, 3) and the intracranial part of the ICA (7). (F) Quantification of the amount of positive staining overlapping with the positive CD31 signal (n = 6–7). Statistical significance was determined by the Friedman test and considered statistically significant if $P < 0.05$.

Vascular Biology (2025) **7** e230013
https://doi.org/10.1530/VB-23-0013

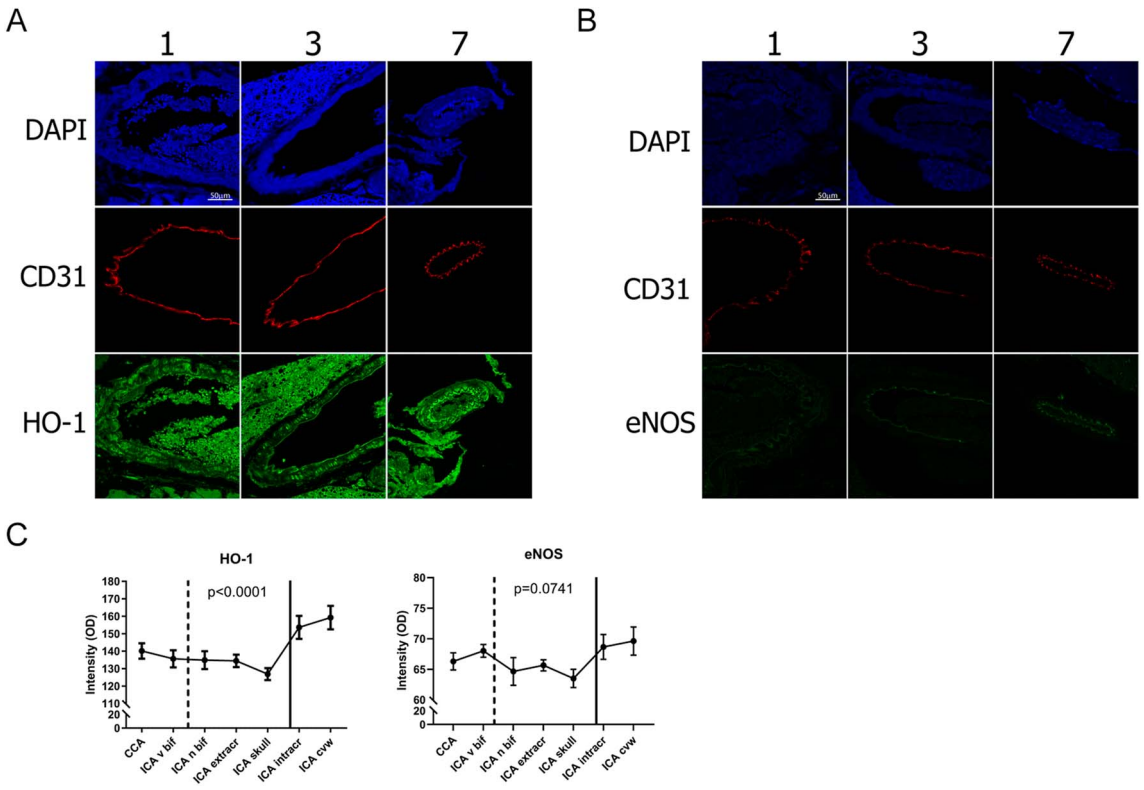

Figure 5

(A, B) Example pictures of changes in (A) HO-1 staining and (B) eNOS staining in 10-week-old ApoE$^{-/-}$ mice on normal chow in the common carotid artery (CCA, 1), the extracranial part of the internal carotid artery (ICA, 3) and the intracranial part of the ICA (7). (C) Quantification of the amount of positive HO-1 and eNOS staining overlapping with the positive CD31 signal (n = 6–7). Statistical significance was determined by the Friedman test and considered statistically significant if $P < 0.05$.

(area fraction SM-MHC/SMA P = 0.0001 and intensity SM-MHC/SMA P = 0.0003), overall leading to no change in differentiation between the intracranial ICA and extracranial CCA and ICA (area × intensity P = 0.0004, post hoc analysis increased expression at point 5 in the skull, but not between extracranial and intracranial segments) (Fig. 3C and D).

The adhesion molecules intercellular adhesion molecule 1 (ICAM-1) and vascular cell adhesion molecule 1 (VCAM-1) regulate the adhesion and transendothelial migration of leukocytes to endothelial cells and thereby facilitate atherogenesis (32, 33). ICAM-1 and VCAM-1 were present in endothelial cells in all examined vessels. ICAM-1 expression in the endothelium was not changed between the different vessel parts (area fraction P = 0.0545 and intensity P = 0.2712) (Fig. 4A and F). VCAM expression, however, increased in the intracranial part of the vessel compared to the extracranial part (area fraction $P < 0.0001$ and intensity P = 0.0006) (Fig. 4B and F).

To investigate paracellular permeability in the intima, the expression of tight junction molecules, such as claudin-5 and ZO-1 were examined. Both stained only weakly in the CCA and ECA, but their presence increased substantially when the vessels passed the skull base (Claudin-5 area fraction $P < 0.0001$, intensity $P < 0.0001$, ZO-1 area fraction P = 0.0006 and intensity P = 0.0005) (Fig. 4C, D, F).

Caveolin is an integral membrane protein that is involved in endocytosis and acts proatherogenic (34, 35). Although the intensity of caveolin in the endothelium showed a significant difference between vessel parts, there was no clear trend toward up- or downregulation in the intracranial vessels compared to the extracranial vessels, and there was no significant difference between the locations in the multiple comparison test (area fraction P = 0.0330 and intensity P = 0.0220) (Fig. 4E).

Antioxidant enzyme expression was determined with a staining for heme oxygenase-1 (HO-1), which is an endogenous antioxidant enzyme highly induced by oxLDL. Its expression increased from the CCA toward the intracranial part of the ICA (area fraction $P < 0.0001$ and intensity $P < 0.0001$). eNOS can increase nuclear NRF2 (36), which is the transcription factor for HO-1. The area of eNOS-positive stained endothelium increased intracranially (area fraction P = 0.0008 and intensity P = 0.0741) (Fig. 5A, B, C).

Vascular Biology (2025) **7** e230013
https://doi.org/10.1530/VB-23-0013

Vessel segment differences were also studied with immunohistochemistry in the intima and media of six 16-week-old C57Bl/6 mice. Also in these young control mice, the number of elastin layers decreased intracranially. In addition, some of the other markers increased: SMA (OD and percent area $P < 0.0001$), Claudin-5 (OD and percent area $P < 0.0001$), HO-1 (ICA (OD $P = 0.0281$ and percent area $P = 0.0039$) and eNOS area (OD $P = 0.0920$ and percent area $P = 0.0071$) (Supplemental Figure 1, Supplemental Table 5).

Endothelial cell characteristics also differ between human intra- and extracranial vessels

The HO-1 gene is known to be protective against atherosclerosis (37, 38). Since eNOS and HO-1 showed a consistent difference between intra- and extracranial artery segments in both ApoE$^{-/-}$ and C57Bl/6 mice, we decided to study the eNOS–NRF2–HO-1 pathway in human intra- and extracranial artery samples. The expression of HO-1, NRF2 and eNOS was compared between the CCA and BA. The fluorescence intensity and positive area of eNOS ($P = 0.002$ and $P = 0.001$) and the fluorescence intensity HO-1 ($P = 0.034$; Fig. 6) were increased in the BA compared to the CCA.

No statistically significant difference was found for the fluorescence intensity of NRF2 ($P = 0.148$), nor for the positive area of HO-1 ($P = 0.756$) and NRF2 ($P = 0.469$). However, for HO-1 to be transcribed, the NRF2 transition from the cytoplasm to the nucleus is more important than total NRF2 levels. Yet, with this staining, the cytoplasmic and nuclear location of NRF2 could not be distinguished.

OxLDL induces protective antioxidant pathways via NRF2 translocation in brain endothelial cells

Based on our immunohistochemical data, we postulate that enhanced levels of antioxidant enzymes protect the intracranial vasculature from atherosclerotic plaque development. To elucidate if the antioxidant response is activated in human brain endothelial cells under pro-atherosclerotic conditions, brain endothelial cells were stimulated with oxLDL, mimicking pro-atherosclerotic conditions. Interestingly, upon treatment of brain endothelial cells with oxLDL, we observed a significant induction of HO-1 mRNA and protein ($P < 0.0001$; Fig. 7A and B). Moreover, oxLDL induced the translocation of the transcription factor NRF2 to the nucleus 4 h after stimulation with oxLDL ($P = 0.0249$; Fig. 7C).

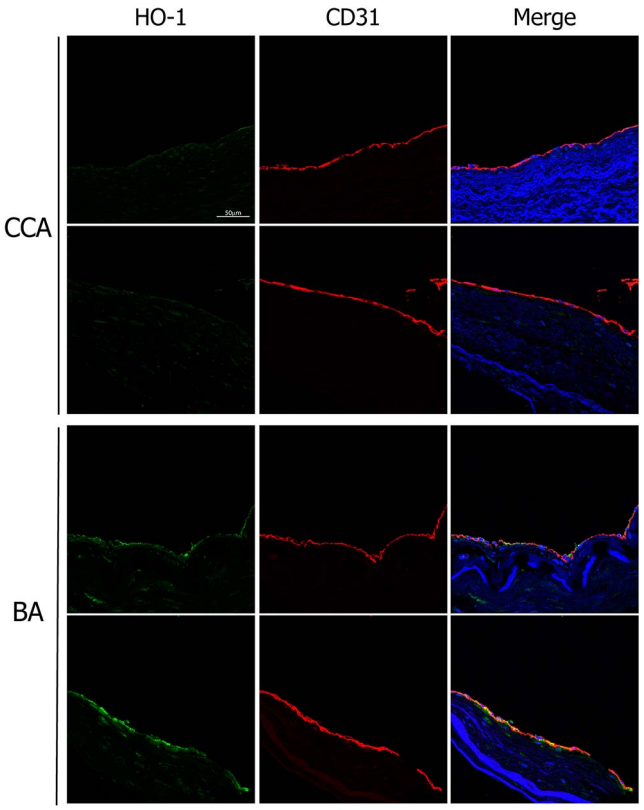

Figure 6

Examples of HO-1 expression in human formalin-fixed paraffin-embedded (FFPE) samples of the common carotid artery (CCA) and basilar artery (BA). (A) HO-1 was labeled with immunofluorescence staining (green), costained with endothelial marker CD31 (red) and counterstained with DAPI (blue) in the CCA and (B) BA (40× magnification).

Discussion

This study demonstrates that multiple mouse models for atherosclerosis do not develop intracranial atherosclerosis despite the presence of moderate or severe extracranial atherosclerotic lesions. Our results indicate a first transition point in atherosclerotic susceptibility at the bifurcation of the ICA and the Ptgpal, after which no atherosclerosis develops in most mice. A second transition point was found at the entry of the ICA into the cranium, after which no atherosclerosis was observed in any of the mice studied. At these transition points, we report morphological differences in the vessel wall, such as reduced elastin layers, an increase in the tight junction protein claudin-5 and an increased expression of the protective antioxidant enzyme HO-1, which may be associated with the observed atheroprotected phenotype of intracranial arteries. These differences seem to be an intrinsic intracranial artery characteristic, as they are present in both 10-week-old ApoE$^{-/-}$ mice before they have developed extracranial atherosclerosis and in young C57bl/6 on normal chow. HO-1 was also increased in human intracranial (BA) samples compared to CCA samples. We also show that human brain endothelial cells increase the expression of HO-1 upon oxLDL stimulation and propose a role for NRF2-mediated HO-1

Vascular Biology (2025) **7** e230013
https://doi.org/10.1530/VB-23-0013

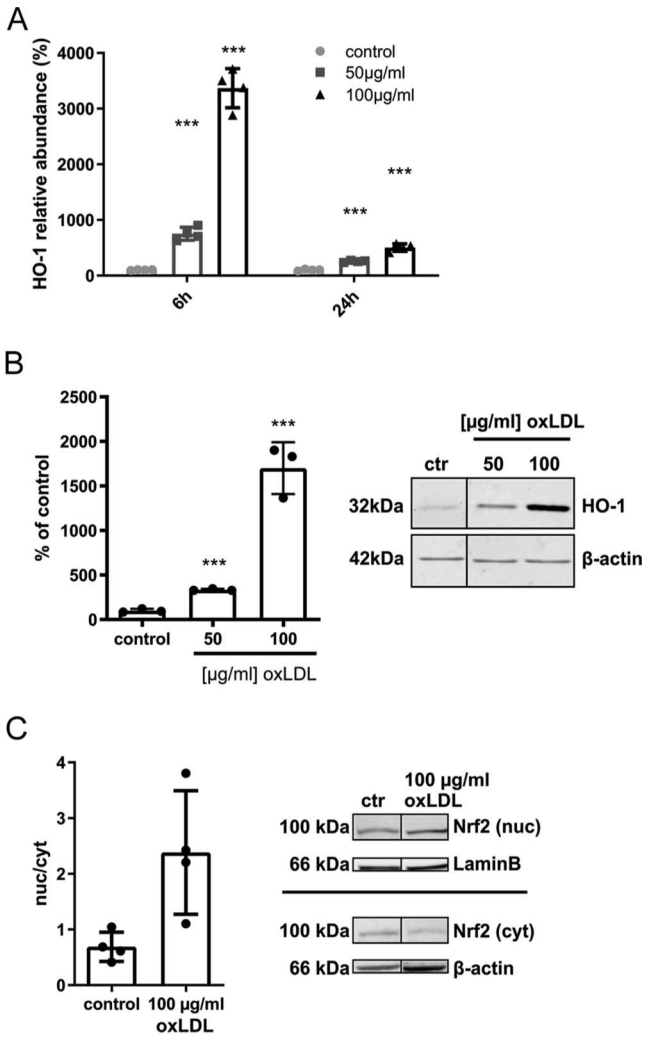

Figure 7

oxLDL protects brain endothelial (hCMEC/D3) cells from oxidative stress. (A) HO-1 expression levels are increased after 6 and 24 h (n = 4). (B) Quantification of HO-1 protein expression as measured by western blot, corrected for actin (n = 3). (C) Western blot analysis of nuclear and cytoplasmic fractions of brain endothelial cells corrected for lamin B and β-actin, respectively, showed an increased nuclear presence of NRF2 (n = 4). Statistical significance was determined by two-tailed Student's t-test. *P < 0.05, **P < 0.001, ***P < 0.0001.

expression in the decreased atherosclerosis susceptibility of intracranial arteries.

Unlike extracranial atherosclerosis, studies on intracranial atherosclerosis are rarely reported in mice. To the best of our knowledge, we are the first group systematically studying the presence of atherosclerosis throughout the ICA in multiple atherogenic mouse models. In ApoE$^{-/-}$ mice of 9 months on chow or high-fat diet, advanced atherosclerotic lesions have been reported in the ECA and ICA (39, 40). The authors, however, only studied the proximal part of the ICA, since dissection of the distal ICA is difficult due to its location between bone structures. We solved this technical problem by decalcifying the entire skull in EDTA for 3–4 weeks and sectioning the entire decalcified skull. Only four other studies have been published on intracranial atherosclerosis in the CoW or its main branches. In ApoE$^{-/-}$LDLr$^{-/-}$ mice of 80 weeks of age on a WD, no atherosclerotic lesions were found in the CoW (18). Intracranial atherosclerosis was also absent in ApoE$^{-/-}$ mice on WD at the age of 29 weeks or at the age of 18 months fed with WD for 6 months (19, 22). Atherosclerosis in the CoW has been reported in male LDLr$^{-/-}$:hApoB$^{+/+}$ mice of 12 months on a chow diet (17). Unfortunately, the actual data are not presented in that paper, and lesion type is not mentioned. We therefore also included male ApoB100/LDLr$^{-/-}$ mice in our study. The absence of intracranial atherosclerosis in the 9-month-old ApoB100/LDLr$^{-/-}$ mice on a high-fat diet could be explained by the younger age of our mice and the difference in ApoB subtype. Yet, the mice in our study were not on normal chow but on a high-fat diet, which accelerates extracranial atherosclerosis. We could not investigate the mice at later time points due to harmful cerebral, inner ear and subcutaneous fat depositions, which occurred without or prior to the formation of foam cells and plaques in intracranial vessels. This indicates that hypercholesterolemia did affect the brain in these mice, but not the vasculature.

Our results suggest that the difference in atherosclerotic susceptibility between extra- and intracranial vessels may be caused by an intrinsic change in vessel wall characteristics and/or endothelial barrier function in intracranial arteries. Brain capillary endothelial cells are highly specialized and are part of the blood–brain barrier (BBB), which has a low permeability to protect the brain from toxic substances, accomplished by the high expression of tight junction markers and selective transporters. Brain-related factors relevant for differentiating endothelial cells into the BBB phenotype may also influence the morphology and reactivity of larger intracranial arteries. For instance, we found an increase in expression of several markers which are important for, but not restricted to, BBB function, such as claudin-5 and ZO-1 in the large intracranial arteries compared to the extracranial part of the ICA. This gradual increase in barrier function can give rise to reduced endothelial barrier permeability and protect the intracranial part of the ICA from lipid accumulation and atherosclerosis development.

Vessel wall differences between extra- and intracranial vessels have only been investigated in a few animal studies. In rabbits, SMC-mediated sensitivity to l-norepinephrine has been shown to differ in different parts of the ICA, marked by an abrupt transition point before its entry through the skull (41). Concanavalin A, which reacts with certain glycocalyx molecules, did not react with the cerebral vessels of rabbits and monkeys but did with the aorta, coronary, femoral and carotid arteries

(42). These differences in vascular response between intra- and extracranial vessels to compounds are probably due to intrinsic differences in vessel wall characteristics, which we also report here. The stimulation of ECs with pro-atherosclerotic compounds such as oxLDL can emphasize these differences. OxLDL stimulates ICAM-1 and VCAM-1 expression in HUVECs and thereby increases monocyte adhesion and plaque formation (43, 44). In rabbits, oxLDL particles impair the contraction and relaxation of carotid arteries, but not of the BA (45). Differences in oxLDL response between extra- and intracranial vessels have also been shown in quails. Interestingly, brain microvascular endothelial cells had a lower death rate in response to oxLDL than carotid endothelial cells (46). This was accompanied by a higher response of antioxidant *HO-1* mRNA and enzyme activity. In human-derived cells, an increase in oxidative stress after oxLDL stimulation has been seen in extracranial endothelial cells such as BAECs and HAECs (47, 48), while a stronger antioxidant defense has been shown in human intracranial arteries compared to extracranial arteries (49). In our experiments, we could link the increased HO-1 mRNA and protein expression in the microvascular endothelial cells to the activation of NRF2, a key player in the regulation of genes involved in vascular antioxidant defense pathways. HO-1 is known for its atheroprotective role, and its induction has been associated with reduced plaque formation in mice (50), while inhibition leads to greater atherosclerotic lesions in rabbits and mice (38, 51, 52). HO-1 deficiency has been shown to lead to hyperlipidemia in humans (53). Increased HO-1 expression has also been associated with a reduction of leukocyte adhesion and monocyte chemotaxis (54, 55, 56). The increased HO-1 expression that we observed in intracranial mouse and human arteries, therefore, suggests a reduced sensitivity to leukocyte adhesion and monocyte chemotaxis. The coinciding increased NQO1 enzyme expression in C57Bl/6 mice is also activated by NRF2 (Supplemental Figure 1) and has likewise been associated with decreased atherosclerosis susceptibility (57, 58). Unfortunately, the IF staining with the NQO1 antibody did not work in the ApoE$^{-/-}$ mice, just like the NRF2 antibody, so it is unclear if the same holds true in ApoE$^{-/-}$ mice. NRF2 must localize to the nucleus in order to induce HO-1 and NQO1 transcription, and nuclear NRF2 can be increased by eNOS (36). An increase in the mRNA levels of *eNOS* has been found in the human intracranial BA compared to the extracranial CCA (8). In this study, we found that there is also an increase in the protein levels of eNOS in both mice and human intracranial vessels. Furthermore, in ApoB100 brain microvasculature, eNOS levels were decreased compared to wild-type mice (59), suggesting that eNOS might be differentially regulated in atherosclerotic models, leading to a higher atherosclerotic susceptibility. Oxidative stress has also been shown to be an important contributor in models of vascular cognitive impairment and dementia (60, 61, 62, 63). In addition, the enhanced expression of tight junctions may further contribute to a reduction in vessel wall permeability, together leading to reduced susceptibility to develop atherosclerosis. Although causality has not been shown yet, changes in elastic layers have also been suggested to influence atherosclerosis vulnerability (64).

A limitation of this study is that from the three genetically modified mouse models we studied, we did not use mice of the same age or the same number of weeks that they were fed on a high-fat diet. The reason for this is that we used animals that were retrospectively harvested from other experimental studies to reduce animal suffering, and because the ApoB100/LDLr$^{-/-}$ mice reached a human endpoint at the age of 37 or 41 weeks. For the immunohistochemistry, we used different analyses in the young ApoE$^{-/-}$ and C57Bl/6 mice to measure endothelial signal only or intima+media signal, respectively. Due to the low amount of slides of some of the measuring points, we were not able to measure the proteins of interest in both models with both methods.

Another limitation of this study is that we used an immortalized brain cell line (hCMEC/D3). Primary cultures of CNS-derived endothelia are phenotypically unstable, undergo rapid cellular senescence and usually fail to develop functional tight junctions, which limits the usefulness of these cells as *in vitro* models of the BBB (27). To overcome these problems, the hCMEC/D3 cell line is transduced several fold. Although the cells retain most of the functional and morphological characteristics of BBB cells, it cannot be excluded that the cells may react differently compared to primary cell lines or endothelial cells *in vivo*.

In conclusion, we report a lack of intracranial atherosclerosis in various atherogenic mouse models up to the age of 41 weeks. These atherogenic mouse models are therefore unsuitable for studying the effects of intracranial atherosclerosis on the development of brain pathology and dementia. Differences in vessel morphology and increased antioxidant capacities in both mice and humans may contribute to the decreased susceptibility to develop atherosclerotic lesions in intracranial arteries. We suggest that HO-1 and its regulation via the NRF2 pathway may play a crucial role in this protective response, since the intracranial vascular expression is increased in both ApoE$^{-/-}$ and C57Bl/6 mice and the human BA.

Supplementary materials

This is linked to the online version of the paper at https://doi.org/10.1530/VB-23-0013.

Declaration of interest

The authors declare that the research was conducted in the absence of any commercial or financial relationships that could be construed as a potential conflict of interest.

Funding

This work was supported by the Netherlands CardioVascular Research Initiative: 'the Dutch Heart Foundation, Dutch Federation of University Medical Centres, the Netherlands Organisation for Health Research and Development and the Royal Netherlands Academy of Sciences' (CVON 2012-06 and CVON 2018-28).

Author contribution statement

DIB, KR, CM, OS, SS, MRM, HJP and OJB helped in data collection, analysis and interpretation of the data. DIB, KR and MJAPD helped in drafting of the manuscript. GRYDM, JCS, LW, HEV and MJAPD helped in revising and editing the manuscript.

Acknowledgements

We thank Dr C Van der Donckt and Dr L Roth of the University of Antwerp for providing ApoE$^{-/-}$ and ApoE$^{-/-}$Fbn1$^{C1039G+/-}$ mouse tissue and Dr P H A Quax and Dr M R de Vries of the LUMC for providing ApoB100/LDLr$^{-/-}$ mouse tissue. We also thank E Suidgeest and I Que for their technical assistance.

References

1 Battistella V & Elkind M. Intracranial atherosclerotic disease. *Eur J Neurol* 2014 **21** 956–962. (https://doi.org/10.1111/ene.12385)

2 Yarchoan M, Xie SX, Kling MA, *et al.* Cerebrovascular atherosclerosis correlates with Alzheimer pathology in neurodegenerative dementias. *Brain* 2012 **135** 3749–3756. (https://doi.org/10.1093/brain/aws271)

3 Roher AE, Tyas SL, Maarouf CL, *et al.* Intracranial atherosclerosis as a contributing factor to Alzheimer's disease dementia. *Alzheimers Dement* 2011 **7** 436–444. (https://doi.org/10.1016/j.jalz.2010.08.228)

4 Suri MF & Johnston SC. Epidemiology of intracranial stenosis. *J Neuroimaging* 2009 **19** (Supplement 1) 11S–6S. (https://doi.org/10.1111/j.1552-6569.2009.00415.x)

5 Ritz K, Denswil NP, Stam OC, *et al.* Cause and mechanisms of intracranial atherosclerosis. *Circulation* 2014 **130** 1407–1414. (https://doi.org/10.1161/circulationaha.114.011147)

6 Weber G. Delayed experimental atherosclerotic involvement of cerebral arteries in monkeys and rabbits (light, sem and tem observations). *Pathol Res Pract* 1985 **180** 353–355. (https://doi.org/10.1016/s0344-0338(85)80105-9)

7 Kurozumi T. Electron microscopic study on permeability of the aorta and basilar artery of the rabbit—with special reference to the changes of permeability by hypercholesteremia. *Exp Mol Pathol* 1975 **23** 1–11. (https://doi.org/10.1016/0014-4800(75)90002-7)

8 Hermkens DMA, Stam OCG, de Wit NM, *et al.* Profiling the unique protective properties of intracranial arterial endothelial cells. *Acta Neuropathol Commun* 2019 **7** 151. (https://doi.org/10.1186/s40478-019-0805-4)

9 Suzuki M. Experimental cerebral atherosclerosis in the dog. I. A morphologic study. *Am J Pathol* 1972 **67** 387–402.

10 Hollander W, Prusty S, Kemper T, *et al.* The effects of hypertension on cerebral atherosclerosis in the cynomolgus monkey. *Stroke* 1993 **24** 1218–1226; discussion 1226-7. (https://doi.org/10.1161/01.str.24.8.1218)

11 Fankhauser R, Luginbuhl H & McGrath JT. Cerebrovascular disease in various animal species. *Ann N Y Acad Sci* 1965 **127** 817–860. (https://doi.org/10.1111/j.1749-6632.1965.tb49447.x)

12 Yamori Y, Horie R, Sato M, *et al.* Hypertension as an important factor for cerebrovascular atherogenesis in rats. *Stroke* 1976 **7** 120–125. (https://doi.org/10.1161/01.str.7.2.120)

13 Yamori Y, Horie R, Sato M, *et al.* Hemodynamic derangement for the induction of cerebrovascular fat deposition in normotensive rats on a hypercholesterolemic diet. *Stroke* 1976 **7** 385–389. (https://doi.org/10.1161/01.str.7.4.385)

14 Ito T & Shiomi M. Cerebral atherosclerosis occurs spontaneously in homozygous WHHL rabbits. *Atherosclerosis* 2001 **156** 57–66. (https://doi.org/10.1016/s0021-9150(00)00622-5)

15 Tu ZL, Yu B, Huang DY, *et al.* Proteomic analysis and comparison of intra and extracranial cerebral atherosclerosis responses to hyperlipidemia in rabbits. *Mol Med Rep* 2017 **16** 2347–2354. (https://doi.org/10.3892/mmr.2017.6869)

16 Shen J, Rastogi R, Guan L, *et al.* Omega-3 fatty acid supplement reduces activation of NADPH oxidase in intracranial atherosclerosis stenosis. *Neurol Res* 2018 **40** 499–507. (https://doi.org/10.1080/01616412.2018.1451290)

17 Drouin A, Bolduc V, Thorin-Trescases N, *et al.* Catechin treatment improves cerebrovascular flow-mediated dilation and learning abilities in atherosclerotic mice. *Am J Physiol Heart Circ Physiol* 2011 **300** H1032–H1043. (https://doi.org/10.1152/ajpheart.00410.2010)

18 Langheinrich AC, Michniewicz A, Bohle RM, *et al.* Vasa vasorum neovascularization and lesion distribution among different vascular beds in ApoE$^{-/-}$/LDL$^{-/-}$ double knockout mice. *Atherosclerosis* 2007 **191** 73–81. (https://doi.org/10.1016/j.atherosclerosis.2006.05.021)

19 Ayata C, Shin HK, Dilekoz E, *et al.* Hyperlipidemia disrupts cerebrovascular reflexes and worsens ischemic perfusion defect. *J Cereb Blood Flow Metab* 2013 **33** 954–962. (https://doi.org/10.1038/jcbfm.2013.38)

20 Kitayama J, Faraci FM, Lentz SR, *et al.* Cerebral vascular dysfunction during hypercholesterolemia. *Stroke* 2007 **38** 2136–2141. (https://doi.org/10.1161/strokeaha.107.481879)

21 Mato M, Ookawara S, Mashiko T, *et al.* Regional difference of lipid distribution in brain of apolipoprotein E deficient mice. *Anat Rec* 1999 **256** 165–176. (https://doi.org/10.1002/(sici)1097-0185(19991001)256:2<165::aid-ar7>3.0.co;2-y)

22 Miller AA, De Silva TM, Judkins CP, *et al.* Augmented superoxide production by Nox2-containing NADPH oxidase causes cerebral artery dysfunction during hypercholesterolemia. *Stroke* 2010 **41** 784–789. (https://doi.org/10.1161/strokeaha.109.575365)

23 Van der Donckt C, Roth L, Vanhoutte G, *et al.* Fibrillin-1 impairment enhances blood-brain barrier permeability and xanthoma formation in brains of apolipoprotein E-deficient mice. *Neuroscience* 2015 **295** 11–22. (https://doi.org/10.1016/j.neuroscience.2015.03.023)

24 Stary HC, Chandler AB, Dinsmore RE, *et al.* A definition of advanced types of atherosclerotic lesions and a histological classification of atherosclerosis. A report from the Committee on Vascular Lesions of the Council on Arteriosclerosis, American Heart Association. *Arterioscler Thromb Vasc Biol* 1995 **15** 1512–1531. (https://doi.org/10.1161/01.atv.15.9.1512)

25 Stary HC, Chandler AB, Glagov S, *et al.* A definition of initial, fatty streak, and intermediate lesions of atherosclerosis. A report from the Committee on Vascular Lesions of the Council on Arteriosclerosis, American Heart Association. *Circulation* 1994 **89** 2462–2478. (https://doi.org/10.1161/01.cir.89.5.2462)

26 Mizee MR, Nijland PG, van der Pol SM, *et al.* Astrocyte-derived retinoic acid: a novel regulator of blood-brain barrier function in multiple

sclerosis. *Acta Neuropathol* 2014 **128** 691–703. (https://doi.org/10.1007/s00401-014-1335-6)

27 Weksler BB, Subileau EA, Perriere N, *et al.* Blood-brain barrier-specific properties of a human adult brain endothelial cell line. *FASEB J* 2005 **19** 1872–1874. (https://doi.org/10.1096/fj.04-3458fje)

28 Livak KJ & Schmittgen TD. Analysis of relative gene expression data using real-time quantitative PCR and the $2^{-\Delta\Delta CT}$ method. *Methods* 2001 **25** 402–408. (https://doi.org/10.1006/meth.2001.1262)

29 Kara F, van Dongen E, Schliebs R, *et al.* Monitoring blood flow alterations in the Tg2576 mouse model of Alzheimer's disease by in vivo magnetic resonance angiography at 17.6 T. *Neuroimage* 2012 **60** 958–966. (https://doi.org/10.1016/j.neuroimage.2011.12.055)

30 Greene EC. *Anatomy of the Rat*, vol 27, p 370. New York: Hafner Pub. Co.

31 Zanellato AM, Borrione AC, Tonello M, *et al.* Myosin isoform expression and smooth muscle cell heterogeneity in normal and atherosclerotic rabbit aorta. *Arteriosclerosis* 1990 **10** 996–1009. (https://doi.org/10.1161/01.atv.10.6.996)

32 Preiss DJ & Sattar N. Vascular cell adhesion molecule-1: a viable therapeutic target for atherosclerosis? *Int J Clin Pract* 2007 **61** 697–701. (https://doi.org/10.1111/j.1742-1241.2007.01330.x)

33 Galkina E & Ley K. Vascular adhesion molecules in atherosclerosis. *Arterioscler Thromb Vasc Biol* 2007 **27** 2292–2301. (https://doi.org/10.1161/atvbaha.107.149179)

34 Rippe B, Rosengren BI, Carlsson O, *et al.* Transendothelial transport: the vesicle controversy. *J Vasc Res* 2002 **39** 375–390. (https://doi.org/10.1159/000064521)

35 Sharma A, Yu C & Bernatchez PN. New insights into caveolae, caveolins and endothelial function. *Can J Cardiol* 2010 **26**(Supp. A) 5A–8A. (https://doi.org/10.1016/s0828-282x(10)71053-9)

36 Wang R, Tu J, Zhang Q, *et al.* Genistein attenuates ischemic oxidative damage and behavioral deficits via eNOS/Nrf2/HO-1 signaling. *Hippocampus* 2013 **23** 634–647. (https://doi.org/10.1002/hipo.22126)

37 Orozco LD, Kapturczak MH, Barajas B, *et al.* Heme oxygenase-1 expression in macrophages plays a beneficial role in atherosclerosis. *Circ Res* 2007 **100** 1703–1711. (https://doi.org/10.1161/circresaha.107.151720)

38 Yet SF, Layne MD, Liu X, *et al.* Absence of heme oxygenase-1 exacerbates atherosclerotic lesion formation and vascular remodeling. *FASEB J* 2003 **17** 1759–1761. (https://doi.org/10.1096/fj.03-0187fje)

39 Seo HS, Lombardi DM, Polinsky P, *et al.* Peripheral vascular stenosis in apolipoprotein E-deficient mice. Potential roles of lipid deposition, medial atrophy, and adventitial inflammation. *Arterioscler Thromb Vasc Biol* 1997 **17** 3593–3601. (https://doi.org/10.1161/01.atv.17.12.3593)

40 Nakashima Y, Plump AS, Raines EW, *et al.* ApoE-deficient mice develop lesions of all phases of atherosclerosis throughout the arterial tree. *Arterioscler Thromb* 1994 **14** 133–140. (https://doi.org/10.1161/01.atv.14.1.133)

41 Bevan JA. Sites of transition between functional systemic and cerebral arteries of rabbits occur at embryological junctional sites. *Science* 1979 **204** 635–637. (https://doi.org/10.1126/science.432670)

42 Weber G, Fabbrim P & Resi L. Lack of endothelial concanavalin A reactivity in the cerebral arteries of rabbits and monkeys. *Atherosclerosis* 1982 **42** 125–128. (https://doi.org/10.1016/0021-9150(82)90133-2)

43 Zhang HP, Zheng FL, Zhao JH, *et al.* Genistein inhibits ox-LDL-induced VCAM-1, ICAM-1 and MCP-1 expression of HUVECs through heme oxygenase-1. *Arch Med Res* 2013 **44** 13–20. (https://doi.org/10.1016/j.arcmed.2012.12.001)

44 Pirillo A, Norata GD & Catapano AL. LOX-1, OxLDL, and atherosclerosis. *Mediators Inflamm* 2013 **2013** 152786. (https://doi.org/10.1155/2013/152786)

45 Napoli C, Paterno R, Faraci FM, *et al.* Mildly oxidized low-density lipoprotein impairs responses of carotid but not basilar artery in rabbits. *Stroke* 1997 **28** 2266–2271; discussion 71-2. (https://doi.org/10.1161/01.str.28.11.2266)

46 Hoekstra KA & Velleman SG. Brain microvascular and intracranial artery resistance to atherosclerosis is associated with heme oxygenase and ferritin in Japanese quail. *Mol Cell Biochem* 2007 **307** 1–12. (https://doi.org/10.1007/s11010-007-9577-4)

47 Zmijewski JW, Moellering DR, Goffe CL, *et al.* Oxidized LDL induces mitochondrially associated reactive oxygen/nitrogen species formation in endothelial cells. *Am J Physiol Heart Circ Physiol* 2005 **289** H852–H861. (https://doi.org/10.1152/ajpheart.00015.2005)

48 Shi Y, Luscher TF & Camici GG. Dual role of endothelial nitric oxide synthase in oxidized LDL-induced, p66Shc-mediated oxidative stress in cultured human endothelial cells. *PLoS One* 2014 **9** e107787. (https://doi.org/10.1371/journal.pone.0107787)

49 D'Armiento FP, Bianchi A, de Nigris F, *et al.* Age-related effects on atherogenesis and scavenger enzymes of intracranial and extracranial arteries in men without classic risk factors for atherosclerosis. *Stroke* 2001 **32** 2472–2479. (https://doi.org/10.1161/hs1101.098520)

50 Juan SH, Lee TS, Tseng KW, *et al.* Adenovirus-mediated heme oxygenase-1 gene transfer inhibits the development of atherosclerosis in apolipoprotein E-deficient mice. *Circulation* 2001 **104** 1519–1525. (https://doi.org/10.1161/hc3801.095663)

51 Ishikawa K, Sugawara D, Goto J, *et al.* Heme oxygenase-1 inhibits atherogenesis in Watanabe heritable hyperlipidemic rabbits. *Circulation* 2001 **104** 1831–1836. (https://doi.org/10.1161/hc3901.095897)

52 Ishikawa K, Sugawara D, Wang X, *et al.* Heme oxygenase-1 inhibits atherosclerotic lesion formation in LDL-receptor knockout mice. *Circ Res* 2001 **88** 506–512. (https://doi.org/10.1161/01.res.88.5.506)

53 Yachie A, Niida Y, Wada T, *et al.* Oxidative stress causes enhanced endothelial cell injury in human heme oxygenase-1 deficiency. *J Clin Invest* 1999 **103** 129–135. (https://doi.org/10.1172/jci4165)

54 Hoekstra KA, Godin DV & Cheng KM. Protective role of heme oxygenase in the blood vessel wall during atherogenesis. *Biochem Cell Biol* 2004 **82** 351–359. (https://doi.org/10.1139/o04-006)

55 Ishikawa K, Navab M, Leitinger N, *et al.* Induction of heme oxygenase-1 inhibits the monocyte transmigration induced by mildly oxidized LDL. *J Clin Invest* 1997 **100** 1209–1216. (https://doi.org/10.1172/jci119634)

56 Hayashi S, Takamiya R, Yamaguchi T, *et al.* Induction of heme oxygenase-1 suppresses venular leukocyte adhesion elicited by oxidative stress: role of bilirubin generated by the enzyme. *Circ Res* 1999 **85** 663–671. (https://doi.org/10.1161/01.res.85.8.663)

57 Hur KY, Kim SH, Choi MA, *et al.* Protective effects of magnesium lithospermate B against diabetic atherosclerosis via Nrf2-ARE-NQO1 transcriptional pathway. *Atherosclerosis* 2010 **211** 69–76. (https://doi.org/10.1016/j.atherosclerosis.2010.01.035)

58 Kim SY, Jeoung NH, Oh CJ, *et al.* Activation of NAD(P)H:quinone oxidoreductase 1 prevents arterial restenosis by suppressing

vascular smooth muscle cell proliferation. *Circ Res* 2009 **104** 842–850. (https://doi.org/10.1161/circresaha.108.189837)

59 Hoyk Z, Toth ME, Lenart N, *et al.* Cerebrovascular pathology in hypertriglyceridemic APOB-100 transgenic mice. *Front Cell Neurosci* 2018 **12** 380. (https://doi.org/10.3389/fncel.2018.00380)

60 Alfieri A, Koudelka J, Li M, *et al.* Nox2 underpins microvascular inflammation and vascular contributions to cognitive decline. *J Cereb Blood Flow Metab* 2022 **42** 1176–1191. (https://doi.org/10.1177/0271678X221077766)

61 Gocmez SS, Sahin TD, Yazir Y, *et al.* Resveratrol prevents cognitive deficits by attenuating oxidative damage and inflammation in rat model of streptozotocin diabetes induced vascular dementia. *Physiol Behav* 2019 **201** 198–207. (https://doi.org/10.1016/j.physbeh.2018.12.012)

62 Jiang P, Chen L, Sun J, *et al.* Chotosan ameliorates cognitive impairment and hippocampus neuronal loss in experimental vascular dementia via activating the Nrf2-mediated antioxidant pathway. *J Pharmacol Sci* 2019 **139** 105–111. (https://doi.org/10.1016/j.jphs.2018.12.003)

63 An L, Shen Y, Chopp M, *et al.* Deficiency of endothelial nitric oxide synthase (eNOS) exacerbates brain damage and cognitive deficit in A mouse model of vascular dementia. *Aging Dis* 2021 **12** 732–746. (https://doi.org/10.14336/ad.2020.0523)

64 Masuoka T, Hayashi N, Hori E, *et al.* Distribution of internal elastic lamina and external elastic lamina in the internal carotid artery: possible relationship with atherosclerosis. *Neurol Med Chir* 2010 **50** 179–182. (https://doi.org/10.2176/nmc.50.179)